Reentry of Ionized Space Debris by Atmospheric Layers with Variable Density

Gabriel Luiz Ferreira Santos[1], Antônio Delson Conceição de Jesus[2]

[1]Department of Astrophysics, National Institute for Space Research, Avenida dos Astronautas, São José dos Campos, 12227-010, São Paulo, Brazil.

[2]Department of Physics, State University of Feira de Santana, Avenida Transnordestina, Feira de Santana, 44036-900, Bahia, Brazil.

ABSTRACT: The atmospheric re-entry of a space object (operational or not) is defined as its return to the surface of the planet. Space Debris can suffer a non-negligible action from atmospheric drag. These bodies tend to initiate the process of natural re-entry. This means that there is no way to avoid a collision of this Space Debris with a commercial aircraft, for example, or change its collision course towards an industrial zone with large amounts of flammable substances stored. The main objective of this work, therefore, is to map the Space Debris families that, after a natural atmospheric re-entry process of up to 2000 seconds (33.33 min) in duration, reach some point in the Washington, DC area and nearby region. Thus, with the survey of Space Debris proposed by this work, the authorities can develop a series of security protocols to maintain the physical integrity of properties, people and aircraft in that region.

KEYWORDS: Space Debris, Atmospheric re-entry, ionized objects, aerodynamics.

1. INTRODUCTION

Planet Earth is surrounded by a cloud of space junk whose constituents are called Space Debris. Most of these bodies originate from space missions. Space Debris arises from human space activities (Human debris - man-made debris) and natural activities (Natural debris - debris generated by nature, rock particles and dust from the main asteroid belt and any other bodies from outer space that are eventually captured by the Earth's gravitational field).

Currently (more than 50 years after Sputnik), with more than 5 thousand launches, space activities are the scene of about 240 explosions, which form the main source of production of Space Debris [1]. In addition to explorations, there are about 2 large collisions per year, involving bodies or stages of higher-stage rockets or spacecraft producing Space Debris. With the current space launch rates, the distribution of these objects in the operational regions increased, even with the action of the atmospheric drag of the objects in LEO (low altitude regions of the Earth).

The Earth's atmosphere is composed of a gaseous mixture spread over five main layers, which extend from the planet's surface to outer space. The atmospheric regions, in order of increasing altitude, are: troposphere, stratosphere, mesosphere, thermosphere and exosphere. This set of gases is attached to the Earth through the terrestrial gravitational attraction.

In this sense, it is necessary to adopt mathematical models that describe the variation of atmospheric density with altitude. Therefore, in this work we chose to use two different models for this parameter in order to compare the accuracy of the final results: the exponential model, given by Equation (1) and the Delhaise model [2], Equation (3).

$$\rho(h) = \rho_0 e^{-\beta h} \tag{1}$$

where β is the altitude factor, ρ is the atmospheric density, h is the height of the Space Debris and ρ_0 is the atmospheric density at sea level. The parameter β can be derived directly from the real roots of the third degree polynomial given by Equation (2):

$$\frac{\mathcal{M}}{4\pi\rho_0 R_e^2}\beta^3 - \beta^2 - \frac{2}{R_e}\beta - \frac{2}{R_e^2} = 0 \tag{2}$$

where M is the mass of the Earth's atmosphere and R_e is the radius of the Earth.

$$\rho = \rho_o \left(\frac{R-s}{R_o-s}\right)^{\tau} \tag{3}$$

where ρ_o is the initial atmospheric density calculated at the perigee point

that has distance R_o from the center of the Earth, τ and s are adjustable parameters. The parameters s and τ can be adapted to estimate observations of solar activities and update the constantly changing dynamics of the atmosphere. In this work

we used s = 0, which indicates that we do not have corrections in solar activities and the value of τ equals -3 which represents the exponential density model frequently used.

In addition to the Earth's gravitational pull, we also consider other perturbative effects relevant to the natural reentry process of Space Debris, such as: the fictitious Coriollis and centrifugal forces; pressure gradient force; aerodynamic force and the magnetic force due to the movement of Space Debris along the Earth's magnetic field.

The unit vectors (i, j, k) form the basis of the geographic coordinate system:

latitude (ϕ); longitude (θ) and altitude (h = r R_e). Figure (1) presents the geometric arrangement of this reference system in relation to the geocentric (x, y, z) coordinates.
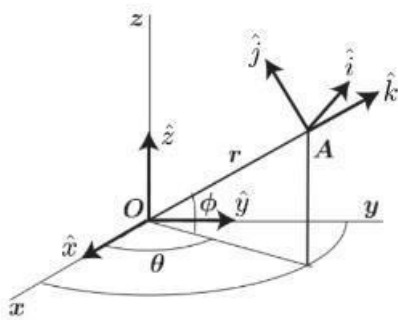
Fig. 1 Atmospheric reference system based on the coordinates (r, θ, φ). And the geocentric reference system, given by the coordinates x, y and z. Adapted from S. Widnall and J. Peraire, MIT.

The mathematical models used in the computer simulations for the Coriollis and centrifugal forces due to the Earth's rotation, the pressure gradient force, the aerodynamic force and the geomagnetic force.

The fictitious forces due to the Earth's rotation, Coriollis and centrifugal, are given by:

$$\vec{a}_{cr} = \omega^2 r \cos^2(\phi)\hat{k} - \omega^2 r \cos(\phi)\sin(\phi)\hat{j} \qquad (4)$$

$$\vec{a}_{cf} = 2\omega[(v\sin(\phi) - w\cos(\phi))\hat{i} - u\sin(\phi)\hat{j} + u\cos(\phi)\hat{k}] \qquad (5)$$

where u, v, w are the components of the velocity vector of the spatial debris
in the geographic coordinate system, that is, u represents the *zonal* component,
v the *meridional* component and w the vertical component.

The pressure gradient force is given by:

$$\vec{a}_{pg}(r, \phi) = \frac{g_0 R_e^2}{r^2}[1 - 4\cos^2(\phi)]\hat{k} - \left[\frac{2g_0 R_e^2 \cos(\phi)\sin(\phi)}{r^2}\right]\hat{j}$$

$$-\frac{\mu}{\rho}\left[-\sec(\phi)\cos(2\phi)\sqrt{\frac{g_0 R_e^2}{r^5}} - \sec(\phi)\sqrt{\frac{g_0 R_e^2}{r^5}} - \frac{\cos(\phi)}{4}\sqrt{\frac{g_0 R_e^2}{r}}\right]\hat{i} \qquad (6)$$

where ω is the rotational velocity of the atmosphere, ρ is the atmospheric density, g_0 is the gravitational acceleration at the Earth's surface given by GM/R^2, M is the mass of the Earth, R_e is the radius of the Earth and G is the constant of universal gravitation and the Greek letter μ represents the viscosity of atmospheric air which depends on the temperature and can be calculated using the Sutherland formula given by

$$\mu(T) = \mu_0 \left(\frac{T}{T_0}\right)^{1.5}\left(\frac{T_0 + 198.72}{T + 198.72}\right) \qquad (7)$$

where T is the local atmospheric temperature in Kelvin, T_0 = 273.15 k, μ_0
= 1, 716 $\times$ 10^{-5} kg / m s. In order to describe the change in temperature due to elevation, we used the International Standard Atmosphere model.

Figure (2) shows the arrangement of the aerodynamic force components. Note that the description of the dynamics of this movement is expressed in terms of the angular coordinates (γ) and ψ. The angle (γ) (flight path angle) is defined as the gap between the velocity vector and the plane of the local horizon. For angles above the local horizon plane, the value of γ is positive, and for openings below this plane, γ is negative. The other flight coordinate used in this work is the angle (ψ) (heading angle) which is defined as the gap between the projection of the velocity vector on the local horizon plane and the local parallel of latitude.
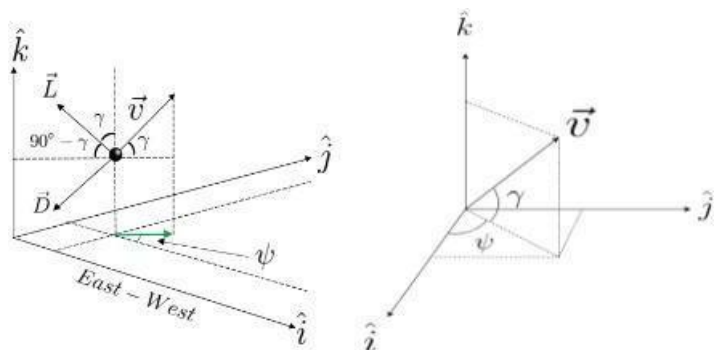
Fig. 2 Definition of flight angles. Note that the heading angle is the angle formed between the projection of the velocity on the local horizon plane and the east-west axis. The two components of the aerodynamic force are also shown in the Figure. The lift component is perpendicular to the velocity vector, and the drag component is antiparallel to the velocity vector.

The aerodynamic force components, drag and lift, are given by:

$$\vec{D} = -\frac{1}{2}\rho \left(\frac{A}{m}\right) C_D v^2 \left[\sin(\gamma)\hat{k} + \cos(\gamma)\sin(\psi)\hat{j} + \cos(\gamma)\cos(\psi)\right.$$

(8)

$$\vec{L} = \frac{1}{2}\rho \left(\frac{A}{m}\right) C_L v^2 \left[\cos(\gamma)\hat{k} - \sin(\gamma)\sin(\psi)\hat{j} - \sin(\gamma)\cos(\psi)\right.$$

(9)

where A is the area of the object perpendicular to the direction of movement; m is its mass; ρ is the atmospheric density where the object is located; the parameters C_D and C_L are coefficients experimentally determined, dependent on the shape of the object and v is the module of the velocity of the body in the atmosphere reference frame.

The physical-mathematical model used to describe the planet's magnetic field is based on data from the thirteenth generation of the International Geomagnetic Reference Field (IGRF-13) [3]. The magnetic force is given by Lorentz formula

$$\vec{F} = Q\vec{v} \times \vec{B} \Rightarrow \vec{a} = \frac{Q}{m}\vec{v} \times \vec{B} \Rightarrow \vec{a}_{mag} = \kappa\vec{v} \times$$

(10) where B⃗ is the Earth's magnetic field where the Space Debris is located, ⃗v is the velocity of the Space Debris, Q is the charge stored on the surface of the Space Debris, and m is your mass. However, it is more convenient to describe this model through the so-called charge-to-mass ratio of the re-entrant Space Debris, here represented by the Greek letter kappa (κ).

2. RESULTS

We simulated dynamics considering the main forces that can act during the process of natural reentry of Space Debris. We were able to elaborate a direct application, whose main objective was to map and detect non-operational space objects with an immediate non-negligible tendency to initiate the process of natural atmospheric re-entry. We selected a region Earth's surface as a possible target for the re-entrant Space Debris.

Figure (3) shows a map of the chosen region, which is clearly denoted by the transparent rectangle. Note that this is Washington, DC and its immediate vicinity, plus the fact that in the lower right corner of the rectangle is an air force base, with constant traffic of military aircraft.
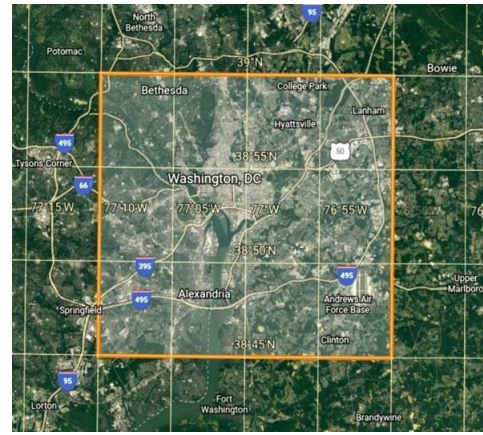

Fig. 3 Space Debris falls area. *Google Earth*.

At this point, we were able to create a map with the distribution of the space junk cloud whose constituents reach some point in the region shown in the Figure (3) in up to 2,000 seconds (about 33 minutes). The Figure (4) shows the projection in the xy plane of the positions of the cataloged Space Debris. The color code used refers to the z coordinate of the bodies. 524 non-operational objects were detected along hyperbolic orbits in operational regions around the Earth (0 km – 36,000 km). Thus, such objects collide very quickly with the Earth and with considerable impact speeds so that the destructive potential increases.
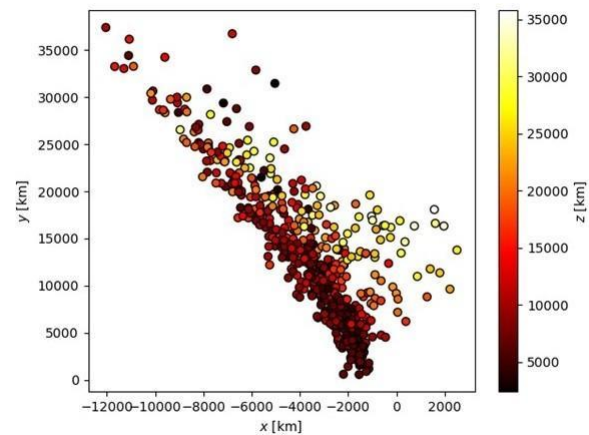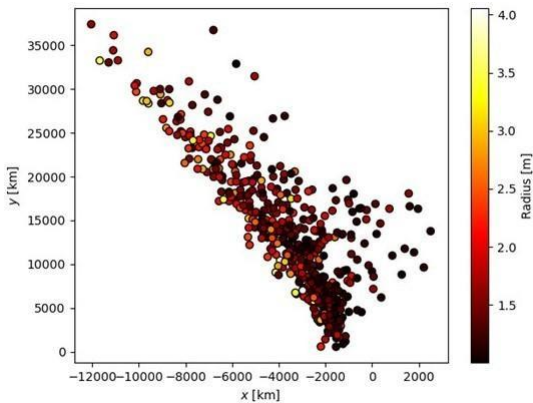

Fig. 4 Projection on the terrestrial equatorial plane of the positions of the 524 cataloged Space Debris. The color bar provides the z coordinate value of each object present in the survey.

Next, we studied the spatial distribution of the identified objects as a function of some physical parameters (mass, radius and charge-to-mass ratio). Figures (5), (6) and (7) show how such properties associated with survey bodies influence their position along the debris cloud mapped by the simulation.
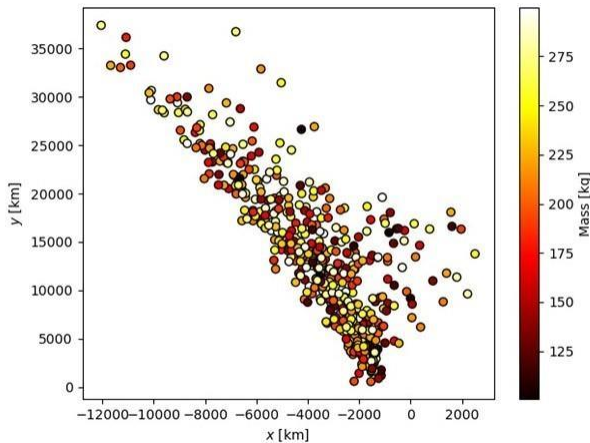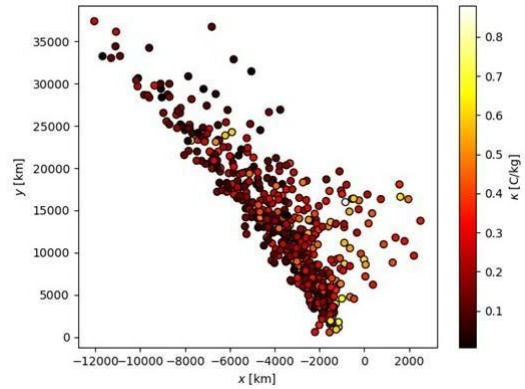
Fig. 5 Projection on the terrestrial equatorial plane of the positions of the 524 cataloged Space Debris. The color bar provides the mass value of each object present in the survey.

Figure (6) shows an equatorial terrestrial plane projection of the position of each Space Debris cataloged at t = 0. The colors refer to their radius. We can get a sense of how the sizes of these cataloged objects are spread across the entire simulated cloud.


Fig. 6 Projection on the terrestrial equatorial plane of the positions of the 524 cataloged Space Debris. The color bar provides the radius value of each object present in the survey.

The Figure (7) presents the distribution of the values of the load-to-mass ratio of the elements belonging to the survey. This parameter is crucial to determine the effect of the interaction of the re-entrant space debris with the Earth's magnetic field.

Fig. 7 Projection on the terrestrial equatorial plane of the positions of the 524 cataloged Space Debris. The color bar provides the value of the load-to-mass ratio of each object present in the survey.

Subsequently, we evaluated the flight coordinates (flight-path angle, heading angle and orbital velocity) of each object in the cloud. Figure (8) shows the scatterplot containing such information necessary to describe the flight dynamics at t = 0. These coordinates can be used to map the direction of the velocity vector of each debris (in principle for any instant of flight). Further- more, the flight angles provide a description of the attitude movement of each object present in the cataloged cloud.
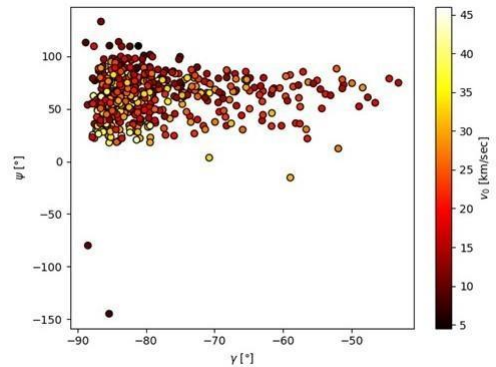
Fig. 8 Flight angles as a function of orbital velocity at t = 0 for each element of the non- operational object family.

In addition, we also elaborated an analysis of the orbits of each of the Space Debris present in this survey. This study was directed through the Keplerian elements associated with each object. Thus, Figures (9), (10) and (11) present the distribution of the orbital elements of each of the Space Debris.
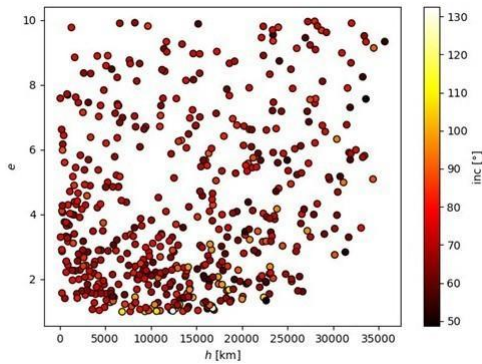
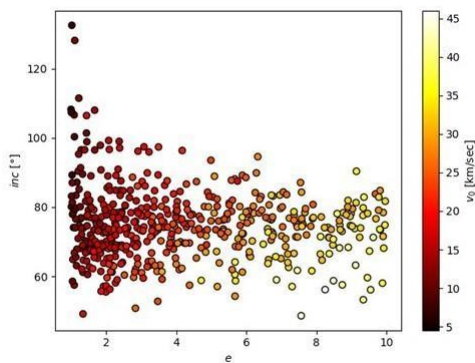**Fig. 9 Orbital altitude, eccentricity and inclination of the identified objects.**

Fig. 10 Eccentricities and inclinations of the orbits in line with the initial orbital velocity.
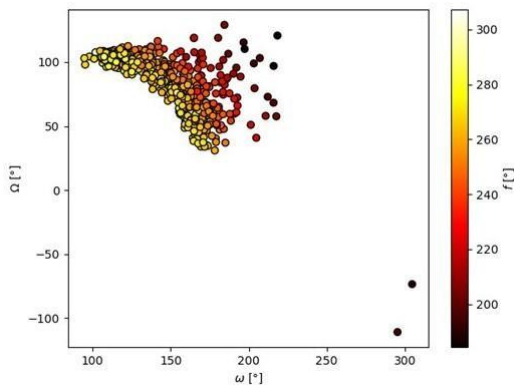

Fig. 11 Euler angles of the orbits of the identified non-operational objects. Source: the author.

Finally, we simulated the atmospheric reentry of a Space Debris whose structure is disintegrated by means of the action of atmospheric drag. Figure (12) is composed of a map showing the locations of each of the shards generated by the fragmentation process.
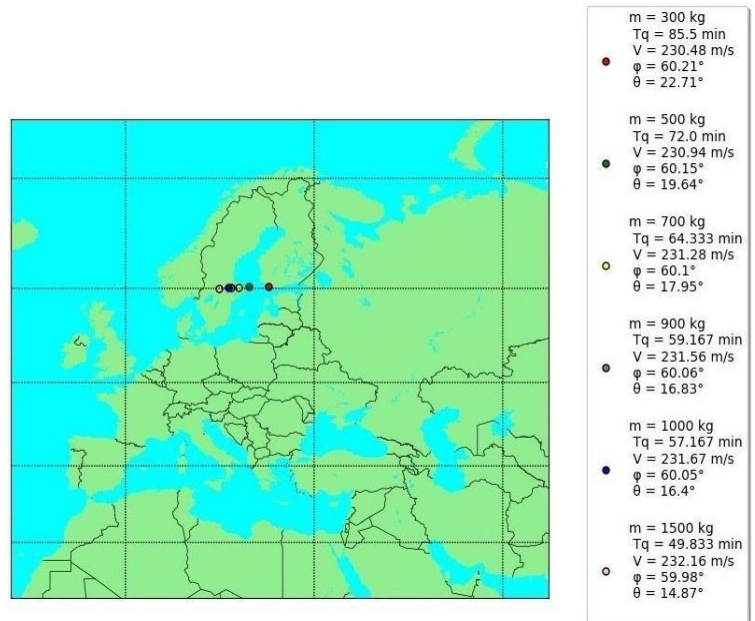

Fig. 12 Fall locations for each Space Debris.

3. METHODS

The Equations of motion were numerically integrated using REBOUND [4]. REBOUND is a direct result of Professor Rein's work and constitutes an indispensable tool for the elaboration of this work. REBOUND is an API (Application Programming Interface) that enables the simulation of the N-body problem (Rein and Liu, 2012, Rein and Spiegel, 2015). This tool also allows the use of several different integrators to solve the equations of motion obtained from the approach to the N-body problem.

Thus, the methodology that permeates this entire study is based on the following steps:

· 1) Find the mathematical models that describe the non-gravitational effects of the study;
· 2) Write all vectors in the geocentric coordinate system;
· 3) Use the expression for Newton's second law to obtain the equations of
   motion associated with the particles of the system;
· 4) Solve the equations of motion by applying REBOUND;
· 5) Develop interest diagrams capable of presenting the main results obtained;
· 6) Discuss and interpret the conclusions generated from the detailed analysis
   of the diagrams produced.

This algorithm faithfully summarizes the entire process that gave rise to all the results of this work.

4. DISCUSSION

Figure (4) is composed of a simplified scatterplot. Note that the debris cloud extends across all operational regions around the Earth. Also, note that most objects have a plane parallel to the Earth's equatorial plane that intersects the Earth's polar

axis at a point below the planet's north pole and above the Earth's equatorial plane. These debris are represented by the darkest red dots on the diagram, that is, whose z coordinate is less than 6371 km.

Thus, all objects cataloged here are found in the northern celestial hemi- sphere. This means that all objects represented by darker red (almost black) dots would be better observed and cataloged by observatories located in the Earth's northern hemisphere. The more yellowish or whitish objects are much further away from the planet's surface so that their detection and subsequent insertion in the Space Debris catalogs become more complicated. In this case, it would be necessary to monitor these bodies through space telescopes specialized in the observation of space debris.

To generate this Space Debris catalog, we did not consider the phenomenon of fragmentation, however all Space Debris are ionized. In this sense, when the process of atmospheric re-entry begins, the object is subject to the action of all the previously mentioned forces. The fragmentation study was carried out separately.

There is a predominance of yellowish dots in the scatterplot of Figure 5. This means that most of the identified objects have a mass greater than 200 kg. In addition, it is also noted that there is a variety of values for the relative distance between the object and the Earth's surface. Therefore, most Space Debris must have high orbital speeds (greater than 30 km/sec) so that their trajectories around the Earth are very eccentric hyperbolas. Also note that few objects have a mass very close to 300 kg.

Figure (6) shows the scattering diagram of the debris along the equatorial plane of the Earth as a function of the size of the objects. It is possible to notice that most of the objects belonging to the survey have a radius of less than 1.5m. Furthermore, it is worth noting that there is a greater amount of Space Debris in MEO. In this sense, these non-operational objects can be more easily observed because they do not have a size on the scale of a few centimeters and are not so far from the Earth's surface. Of course, larger debris that is located in LEO has a greater chance of being measured by ground-based observatories. However, as most of them have a radius of less than 2 m and are located in MEO, the number of objects effectively identified by the detectors would be considerably reduced by the conjuncture of these last facts. This means that to increase the chance of measurement, space agencies should launch satellites equipped with sensors capable of detecting the smallest non-operational objects, so the effective cost to validate and prove the existence of such objects would be very high.

Note that there are a small number of objects in Figure (7) whose charge- to-mass ratio is close to 1 C/kg for each unit of mass. This is because few Space Debris from this set have a small mass (less than 200 kg in this case). Therefore, few objects suffer a more expressive action of the Earth's magnetic field. This fact directly influences the final position

and spatial arrangement of the debris cloud in this survey.

In other words, the values for the declination coordinate of the elements in this catalog are not so high that the object's plane parallel to the terrestrial equatorial plane touches the Earth's polar axis at a point superior to the planet's north pole. In this sense, the interpretation provided earlier through the Figure (7) becomes more evident when we analyze more carefully the contribution of the magnetic interaction between the ionized debris and the Earth. All 524 objects have a certain amount of charge stored on their surface. It is also worth highlighting the fact that the range of values for the charge-to-mass ratio of the cloud elements is in agreement with the processes of ionization of space objects through interaction with the terrestrial atmosphere, since such values would be higher. if we considered a spatial distribution closer to the Earth's surface, the air density would be greater and this would con- tribute to a much more expressive electrification than the case considered in this work. Of course, this last statement would not be true if we considered the perturbation of solar radiation, since this effect also contributes to the increase in the charge-to-mass ratio of space objects.

Flight angles provide the direction of body movement. Note that all cataloged cloud debris has a negative value for the flight-path angle, Figure (9). This means that the altitude of all of them has a negative temporal rate, which was expected, since these objects are at the beginning of the atmospheric re-entry process.

The heading angle (vertical axis) tells you where the body is heading in relation to the Earth's surface. Most of the objects present in this survey have a positive value between approximately $20°$ and $100°$ for this parameter. This means that a considerable number of Space Debris is heading towards the northeast, north or northwest.

Also note that there are two isolated dots at the bottom of the diagram. These two particular debris are heading towards the southeast or southwest directions. The object whose heading angle is close to $60°$ or $70°$ (top point) is moving to the southeast direction. And the debris velocity vector represented by the lowest point with heading angle close to $150°$ points to the southwest direction. Although both have a flight-path angle close to $90°$, their altitude decay rates are not the highest in the cloud, as these debris have a low orbital velocity compared to the other elements in the cloud.

This happened precisely because we fixed the falling time of objects at up to 33 minutes. Thus, objects with a lower velocity and which are to the east of the impact zone must have a more direct trajectory to reach some point in the region during this period. Also note that there are other objects with a low velocity, however with a heading angle practically opposite to that of these debris (upper region of the diagram), this fact reveals the interference of the initial position of the debris in the cloud in its natural re-entry trajectory. In short,

very few objects in the catalog have direct trajectories, most objects have curvilinear trajectories until they reach some place in the Washington region. This increases the risk of possible collisions throughout the re-entry process, as the more complex the route, the greater the chance of a collision occurring.

Regarding the orbital speed of these objects, we can say that most is located in the range of 5 km/s to about 25 km/s (reddish or almost black spots). Next, the most common speed value is between 25 km/s and 30 km/s (orange dots). Debris whose speed is greater than 30 km/s form the minority of the cloud. However, all constituents of the survey have sufficient orbital speed to move along hyperbolic trajectories around the planet.

The Figure (9) lists important parameters regarding the description of the orbit of the constituents of this catalog. The vertical axis shows the values of the orbital eccentricities of each element in the group. As stated earlier, all objects move along hyperbolic trajectories due to their high orbital speeds. In addition, the horizontal axis informs the relative distance between the object and the Earth's surface. Note that altitudes vary so these objects are spread across three major operational regions around Earth: LEO; MEO and GEO. To generate this catalogue, we took care to reformulate the dynamics of each region in order to consider only the main forces acting in each orbital band. It is also worth noting that most objects have an orbital inclination close to 90°, a fact that can be corroborated by the previously provided interpretation of planes parallel to the terrestrial equator. This is evident when we notice that most of the points have a reddish color.

Note that the values for the eccentricity are between 1 and 10, which means that the orbits described by the objects are open (parabolas or hyperbolas). It is also worth noting that all the debris is scattered throughout all operational orbital regions around the Earth.

Finally, note that none of the trajectories takes place along the terrestrial equatorial plane. This indicates that there is a considerable chance that these objects came from other regions of the Solar System, such as the Main Asteroid Belt, since fragments of asteroids from the main belt or small objects from the outermost regions of the solar system have closed orbits with high eccentricities (close to 1) with a non-zero orbital inclination [5]. As such closed trajectories are extremely flat ellipses (0.80 e < 1), we can consider their path along the solar system plane to be a hyperbola. Therefore, in practice, cataloged objects can encompass these types of natural debris coming from the depths of the Solar System.

Figure (10) relates the orbital eccentricity with the inclination of the orbit plane and the object's velocity. Note that the slower objects (more reddish or black) have the smallest eccentricities and are spread over orbital planes, whose inclination varies from about 50° to 130°. So this gives us an idea of how the Space Debris cloud disperses across the

northern celestial hemisphere. To understand in a more precise way the spatial arrangement of objects, we created the diagram in Figure (11), which relates the Euler angles of the debris. These openings are: the longitude of the ascending node (Ω); the periastro argument (ω) and the true anomaly (f).

Figure (11) informs how the trajectory is arranged along the orbital plane and in which sector of the orbit the object is. We can infer from the diagram that practically all the debris is located in octants 1 and 2. This fact can also be deduced from the Figure (5), since almost all the debris has a negative value for the its x coordinate, while y and z are all positive.

Another important effect that we can extract from Figure (11) is the fact that the higher the values of the ascending node longitude and the periastron argument, the greater the true anomaly of the debris. This means that there is a chance that some debris will start its re-entry process at some point in the seventh or third octant. This feature must be taken into account in the study of atmospheric reentry trajectories, as this allows estimating which positions on the Earth's surface will be flown over by objects during the reentry process. Note that in Figure (12) there is a legend with the masses of the fragments, their fall times, their impact velocities and the geographic coordinates (latitude and longitude) of the impact site. We can see three patterns from the values of such quantities: 1) the more massive the fragment, the shorter the fall time; 2) the greater the mass of the shrapnel, the greater the impact velocity; 3) the locations of the Space Debris falls are arranged, practically, along the parallel of latitude 60°.

The fact that the time of fall is inversely proportional to the mass of the fragment can be explained from the analysis of the effect caused by the aero- dynamic force. Note that the greater the mass, the smaller the area-to-mass ratio of the fragment, which causes the intensity of the aerodynamic force to decrease.

On the other hand, the intensity of the gravitational attraction between the fragment and the planet Earth increases if the mass grows so that the impact velocity becomes more expressive. Finally, note that the less massive fragments have a greater longitude (they are located further to the right on the map), this is precisely because the body spends more time interacting with the atmosphere so that its zonal displacement increases.

5. CONCLUSION

The concept of natural reentry of Space Debris was also presented through- out this work. We define the natural reentry of Space Debris as a spontaneous phenomenon that happens because of the drag component of the aerodynamic force. In summary, one of the main conclusions of this study on atmospheric re-entry was the fact that debris with a higher charge-to-mass ratio tends to reach points at higher latitudes along the Earth's surface. This effect is caused by a stronger

interaction with the Earth's geomagnetic field. In addition, we also studied the phenomenon of Space Debris fragmentation. The main characteristic observed was the fact that the pieces spread along the same parallel latitude. This is due to the significant increase in atmospheric density with decreasing altitude of the space debris. Thus, the more massive fragments, in general, have a shorter flight time than the lower-mass debris as shown in Figure (12).

The main objective here was to present a particular cloud of Space Debris that share among themselves the fact of reaching some point in the Washing- ton, DC region in a maximum time of 33 minutes. Therefore, all the results of this chapter reflect the elaboration of a survey of ionized Space Debris that can reach some point in this zone (see Figure 3). Note, therefore, that this family of Space Debris generated by the computer simulation has 524 space debris whose movement is along orbits whose eccentricity is greater than or equal to 1. This is due to the fact that these bodies must reach the Earth's surface quickly so your orbital velocity distribution at $t = 0$ s must have high values (something on the order of a few tens of kilometers per second).

Therefore, with the survey of Space Debris proposed by this work, the authorities are able to take all the necessary mitigation measures to prevent any physical damage to people or their property from occurring in the region of the American capital, that is, they enable them to develop a series of security protocols to maintain the physical integrity of property, people and aircraft (commercial and military) present in that region.

REFERENCES

1. Klinkrad, H.: Space debris mitigation activities at esa in 2013. Technical Presentation delivered at the 51st session of the UNCOPUOS STSC, UN Office in Vienna **14** (2014)

2. Delhaise, F.: Analytical treatment of air drag and earth oblateness effects upon an artificial satellite. Celestial Mechanics and Dynamical Astronomy **52**(1), 85–103 (1991)

3. Alken, P., Th´ebault, E., Beggan, C.D., Amit, H., Aubert, J., Baerenzung, J., Bondar, T., Brown, W., Califf, S., Chambodut, A., *et al.*: International geomagnetic reference field: the thirteenth generation. Earth, Planets and Space **73**(1), 1–25 (2021)

4. Rein, H., Liu, S.-F.: Rebound: an open-source multi-purpose n-body code for collisional dynamics. Astronomy & Astrophysics **537**, 128 (2012)

5. Sheppard, S.S., Trujillo, C.: New extreme trans-neptunian objects: toward a super-earth in the outer solar system. The Astronomical Journal **152**(6), 221 (2016)